Stem Cell Research (2012) 9, 143–155

Available online at www.sciencedirect.com

SciVerse ScienceDirect

www.elsevier.com/locate/scr

REGULAR ARTICLE

Neuroprotective effects and magnetic resonance imaging of mesenchymal stem cells labeled with SPION in a rat model of Huntington's disease

Louise Moraes [a, b], Andreia Vasconcelos-dos-Santos [a, b], Fernando Cleber Santana [a, b], Mariana Araya Godoy [a, b], Paulo Henrique Rosado-de-Castro [a, c, d], Jasmin [a, b], Ricardo Luiz Azevedo-Pereira [a, b], Wagner Monteiro Cintra [a, e], Emerson Leandro Gasparetto [a, c], Marcelo Felippe Santiago [a, b], Rosalia Mendez-Otero [a, b, d,*]

[a] *Centro de Ciências da Saúde, Instituto de Biofísica Carlos Chagas Filho, Universidade Federal do Rio de Janeiro, Brazil*
[b] *Programa de Terapias Celulares — PROTECEL, Universidade Federal do Rio de Janeiro, Brazil*
[c] *Departamento de Radiologia, Universidade Federal do Rio de Janeiro, Brazil*
[d] *Instituto Nacional de Biologia Estrutural e Bioimagem (INBEB), Brazil*
[e] *Instituto de Ciências Biomédicas — Centro de Ciências da Saúde, Universidade Federal do Rio de Janeiro, Brazil*

Received 7 March 2012; received in revised form 26 April 2012; accepted 18 May 2012
Available online 29 May 2012

Abstract Bone marrow mesenchymal stem cells (MSC) have been tested and proven effective in some neurodegenerative diseases, but their tracking after transplantation may be challenging. Our group has previously demonstrated the feasibility and biosafety of rat MSC labeling with iron oxide superparamagnetic nanoparticles (SPION). In this study, we investigated the therapeutic potential of SPION-labeled MSC in a rat model of Huntington's disease, a genetic degenerative disease with characteristic deletion of striatal GABAergic neurons. MSC labeled with SPION were injected into the *striatum* 1 h after quinolinic acid injection. FJ-C analysis demonstrated that MSC transplantation significantly decreased the number of degenerating neurons in the damaged *striatum* 7 days after lesion. In this period, MSC transplantation enhanced the striatal expression of FGF-2 but did not affect subventricular zone proliferation, as demonstrated by Ki67 proliferation assay. In addition, MSC transplantation significantly reduced the ventriculomegaly in the lesioned brain. MRI and histological techniques detected the presence of the SPION-labeled cells at the lesion site. SPION-labeled MSC produced magnetic resonance imaging (MRI) signals that were visible for at least 60 days after transplantation. Our data highlight the potential of adult MSC to reduce brain damage under neurodegenerative diseases and indicate the use of nanoparticles in cell tracking, supporting their potential as valuable tools for cell therapy.

* Corresponding author at: Instituto de Biofísica Carlos Chagas Filho, Centro de Ciências da Saúde, Sala G028, Cidade Universitária, 21941-590, Rio de Janeiro, Brazil.
E-mail address: rmotero@biof.ufrj.br (R. Mendez-Otero).

1873-5061/$ - see front matter © 2012 Elsevier B.V. All rights reserved.
doi:10.1016/j.scr.2012.05.005

Introduction

Huntington's disease (HD) is a progressive, fatal and neurodegenerative disorder produced by CAG trinucleotide expansion in exon 1 of the gene coding for the huntingtin protein (htt) (The Huntington's Disease Collaborative Research Group, 1993). Despite the widespread expression of htt in the brain and the body, expression of mutant htt leads to the selective death of the medium-size spiny GABAergic neurons in the *striatum* (Cowan and Raymond, 2006; Sieradzan and Mann, 2001; Subramaniam et al., 2009), resulting in the appearance of generalized involuntary movements. Excitotoxicity is suggested to be involved in the pathogenesis of HD and intrastriatal injection of quinolinic acid (QUIN), an agonist of the N-methyl-D-aspartic acid receptor, induces a similar pattern of neuronal death (Estrada Sanchez et al., 2008).

MSC transplantation has been found to produce improvements in several disease neurodegenerative models, including Alzheimer's disease (Lee et al., 2010), amyotrophic lateral sclerosis (Kassis et al., 2008) and acid sphingomyelinase deficiency (Jin et al., 2002). MSC-mediated neuroprotection is often associated with their anti-inflammatory effects (Ohtaki et al., 2008) and/or secretion of growth factors (Caplan and Dennis, 2006), which might serve to inhibit disease progression (Le Blanc and Ringden, 2007; Uccelli et al., 2007). The neuroprotective properties of MSC raise the possibility of developing a therapy to prevent or retard the degeneration of vulnerable striatal neuronal populations in HD, which could be a more feasible approach than neuronal replacement in a clinical scenario.

The increasing number of studies focusing on regenerative medicine and stem cell transplantation is being accompanied by the development of techniques using many types of nanoparticles. The combination of nanotechnology with stem cell research may be able to address some challenges in this research field, including stem cell monitoring after transplantation. Since most experimental cell-tracking techniques require histological analysis, non-invasive approaches to assess migration, fate and integration of transplanted cells represent a significant advance for the clinical application of biomedical treatments using stem cells. MRI of magnetically labeled cells is an emerging technology that offers excellent resolution in vivo. SPION are negative contrast agents that render transplanted stem cells trackable when imaged with the appropriate pulse sequence. These nanoparticles consist of magnetite (iron oxide) cores, which are coated with dextran or siloxanes encapsulated by a polymer or further modified to facilitate internalization (Jung and Jacobs, 1995; Rogers et al., 2006).

Our group has recently shown that SPION-labeling does not affect viability, proliferation and differentiation of MSC (Jasmin et al., 2010) and we have now applied the same technique to track MSC in vivo in a rat model of Huntington's disease. Moreover, to investigate the neuroprotective potential of MSC in HD it is important to evaluate the effect before massive cell death. In this report, we implanted SPION-labeled MSC into the *striata* of rats 1 h after QUIN injection, to investigate their neuroprotective effects and to monitor their fate over the long term.

Methods

Cell culture

To obtain bone marrow cells, tibias and femurs were isolated from Wistar rats, the epiphyses were removed, and the bones were individually inserted in 1 mL automatic pipette polypropylene tips and then placed in 15 mL tubes. The bones were centrifuged at 300×*g* for 1 min and the pellets suspended in Dulbecco's modified Eagle's medium F-12 (DMEM F-12; Invitrogen Inc., Carlsbad, CA, USA), supplemented with 10% fetal bovine serum (FBS; Invitrogen Inc.), 2 mM L-glutamine (Invitrogen Inc.), 100 U/mL penicillin (Sigma-Aldrich Co., St. Louis, MO, USA), and 100 μg/mL streptomycin (Sigma-Aldrich Co.). Mononuclear cells were purified by centrifugation in Histopaque 1083 (Sigma-Aldrich Co.) gradient at 400×*g* for 30 min. After three washes in phosphate-buffered saline (PBS) using centrifugation at 300×*g*, the cells were plated in 75 cm^2 flasks with supplemented DMEM F-12 and maintained in 5% CO_2 atmosphere at 37 °C. The medium was replaced 48–72 h after initiation of the culture, to remove nonadherent cells, and the adherent cells were grown to confluence before each passage. The medium was replaced three times a week. After a third replating, cultured cells were labeled with SPION.

Labeling and viability of MSC

As described previously (Arbab et al., 2004a, 2004b; Jasmin et al., 2010), a stock solution of protamine chlorhydrate (Valeant Pharmaceuticals International, São Paulo, SP, Brazil) (5 μg/mL) was added to the culture medium at a dilution of 1:1000 and mixed with SPION (Feridex IV, Advanced Magnetics Inc., Cambridge, MA, USA) (100 μg/mL) for 30 min at room temperature on a rotating shaker. This solution containing FE–Pro complexes was added to an equal volume of the culture medium, such that the final concentration of ferumoxides was 50 μg/mL and the final dilution of protamine sulfate was 1:2000. The cell cultures were kept at 37 °C for 4 h in this medium, washed in phosphate-buffered saline (PBS, pH 7.4) trypsinized and transplanted or fixed with 4% paraformaldehyde (PF) for in vitro assays. For viability assays, cells were washed and incubated for 30 min at room temperature with the LIVE/DEAD viability/cytotoxicity kit (Invitrogen Inc.). Due to intracellular esterase activity determined by the enzymatic conversion of cell-permeant calcein to the intensely fluorescent calcein, green fluorescence depicts live cells. Dead MSC show red fluorescence induced by ethidium homodimer, which enters cells with damaged membranes.

Prussian blue staining

For Prussian blue staining, which indicates the presence of iron, cells or mounted sections were washed and incubated for 20 min in 10% potassium ferrocyanide (VETEC) and 20% hydrochloric acid (VETEC). After washing, samples were counterstained with nuclear fast red (VETEC).

Transmission electron microscopy

For electron microscopy, mesenchymal cells were washed in 0.1 M phosphate buffer, pH 7.2, and then fixed with 2% glutaraldehyde and 2% paraformaldehyde in 0.1 M phosphate buffer for 1 h at room temperature. Cells were scrubbed off the bottles with a rubber cell scraper, after being washed three times in PB, and the suspension centrifuged at 250×*g* for 5 min each time. The pellet was then washed twice in 0.1 M cacodylate buffer, pH 7.2 and post-fixed in a solution containing 1% osmium tetroxide and 0.8% potassium ferrocyanide and 5 mM $CaCl_2$ in 0.1 M cacodylate buffer, pH 7.2 for 60 min at room temperature and in the dark. Pellets were cut into small (1–3 mm^3) pieces, dehydrated in acetone, and embedded in Epoxy resin. Thin sections were stained with uranyl acetate for 40 min and lead citrate for 5 min, and observed in a JEOL 1200 microscope operating at 80 kV.

Surgery and Transplantation procedures

Surgeries were performed on 3-month-old male Wistar rats, weighing 300 to 350 g. All experiments were conducted in accordance with the National Institutes of Health Guide for the Care and Use of Laboratory Animals (NIH Publication No. 80-23), and were approved by the Committee for the Use of Experimental Animals of our Institution. Rats were immobilized under ketamine hydrochloride (50 mg/kg, i.p.) and xylazine hydrochloride (10 mg/kg, i.p.) anesthesia and injected bilaterally with 1 μL QUIN 100 nM into the *striata* at the following stereotaxic coordinates: A/P 0.7, M/L −3.0 and D/V −5.0 mm from bregma. After 1 h, cell transplants (5×10^5 or 1×10^6 in 7 μL saline) were made using the same coordinates. Accordingly, the control striata were injected with 7 μL saline. At different time point post-surgery, the rats inhaled a lethal dose of ether and were perfused transcardially with 0.9% saline, followed by a buffered 4% PF solution, and 10% sucrose in PF. The removed brains were immersed in a 30% buffered sucrose solution overnight for cryoprotection, then quickly frozen in liquid nitrogen and cut coronally on a cryostat at 20 μm thickness.

In vivo MRI

Magnetic resonance images were acquired at 1.5-T (Magnetom Avanto, Siemens Medical, Erlangen, Germany) using an 8-channel knee coil. The study protocol consisted of high-resolution T2 weighted sequences in the coronal plane [repetition time (TR) 4000 ms, echo time (TE) 83 ms, matrix 256×112, section thickness 2 mm, NEX 9] and T2* weighted sequences in the sagittal plane (TR 11 ms, TE 4.8 ms, matrix 384×156, section thickness 0.7 mm, NEX 3).

Immunohistochemistry

For immunofluorescence staining, the sections were pre-incubated for 30 min, at room temperature, in a solution containing 10% normal goat serum (Sigma-Aldrich) to block nonspecific binding sites. Sections were then incubated overnight with the primary antibodies in PBS, at 4 °C. The following primary antibodies were used: mouse monoclonal IgG anti-dextran (1:1000, StemCell Technologies, Vancouver, BC) and rabbit monoclonal IgG anti-Ki67 (1:100, Abcam, Cambridge, MA). The secondary antibodies used were, respectively, Alexa 488-conjugated goat anti-mouse IgG (1:1000, Invitrogen) and Cy3-conjugated goat anti-rabbit IgG (1:400, Jackson ImmunoResearch, West Grove, PA). Sections were incubated in the secondary antibodies for 2 h at 37 °C. After rinsing in PBS, the sections were kept for 15 min in a nuclear staining solution with 0.1% DAPI (4,6-diamidino-2-phenylindole, Sigma-Aldrich) and mounted using N-propylgalate mounting medium. Images were acquired using a Zeiss Axiovert 200 M microscope equipped with an Apotome slide and fluorescence optics or a Zeiss LSM 510 META confocal microscope.

FJ-C Staining

FJ-C (Histo-Chem Inc., Jefferson, AR, USA), a specific marker of neuronal death [28, 29] was used to evaluate the extent of neurodegeneration after QUIN injection. Sections were dehydrated in 100% ethanol for 3 min, followed by 1 min in 70% ethanol. After 1 min wash in distilled water, the sections were treated with 0.06% $KMnO_4$ with gentle agitation for 15 min. After washing in distilled water, the sections were placed in a solution composed of 0.001% FJ-C in 0.1% acetic acid for 30 min. The slides were washed three times with distilled water, dried, and coverslipped with DPX mounting medium (Electron Microscopy Sciences, Fort Washington, PA, USA).

Cell counting and ventricular area measurements

FJ-C staining was performed in the lesion core. We counted all FJ-C-positive cells (n=7) in 6 predetermined striatal fields, which included a representative area of the lesion. Coronal sections of the SVZ were chosen along the rostrocaudal axis (+1.00 mm to +0.20 mm from the bregma) using the same anatomical references for both groups, including: olfactory bulb, cortex, corpus callosum, and white matter. In 6 to 8 sections, all immunoreactive cells in the SVZ of the lateral wall of lateral ventricles were counted (except for the dorsolateral SVZ, to exclude migrating cells) including a distance of 60 μm from the ventricular lumen (n=8). The lateral walls were measured using AxioVision software and the values were plotted as the average number of cells/mm ±SEM for each group. To assess ventricular size (n=4), serial coronal sections at different rostrocaudal levels of the brain were photographed, and the border of each ventricle was outlined using AxioVision software. We measured the ventricular area in three rostrocaudal levels: anterior (2.7–1.6 mm distant from the bregma), medial (1.0–0.7 mm distant from the bregma), and posterior (0.26–0.4 mm distant from the bregma).

Immunoblotting assay

Animals (n=4) were killed and the *striata* were carefully dissected in ice-cold 10 mM PBS. Tissues were homogenized in ice-cold lysis buffer (20 mM Tris–HCl pH 7.4; 150 mM NaCl; 2 mM EDTA; 0.2% Triton X-100; 1:1000 of Protease Inhibitor Cocktail Set III [Calbiochem]). Following incubation on ice for 40 min, the lysed cells were centrifuged at 12,000×*g* for

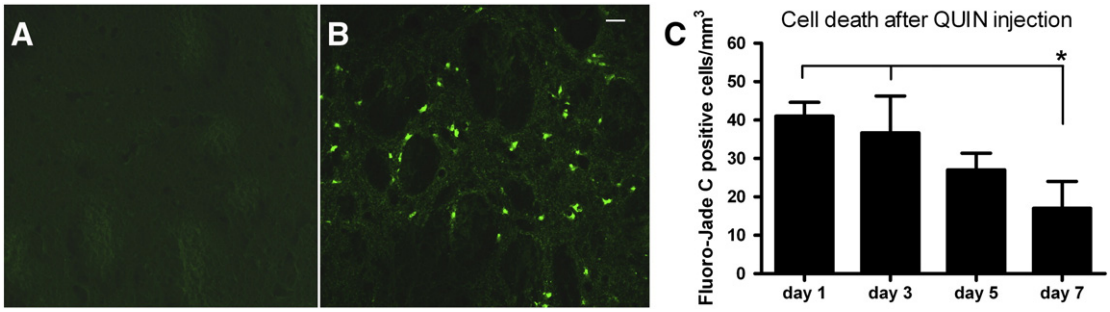

Figure 1 Characteristic feature of a striatal neurotoxic lesion in the *striatum* after QUIN injection. FJ-C positive cells were detected at day 1 after QUIN striatal injection (B), but not in the *striatum* injected with saline (A). Graph shows the quantification of FJ-C positive cells in *striata* (C). Neurodegeneration was observed from day 1 to day 7 post-injection, and staining at different time points after QUIN injection was significantly higher at 1–3 d (*$p<0.05$, one-way ANOVA followed by Tukey's test). Scale bar: A and B = 20 μm.

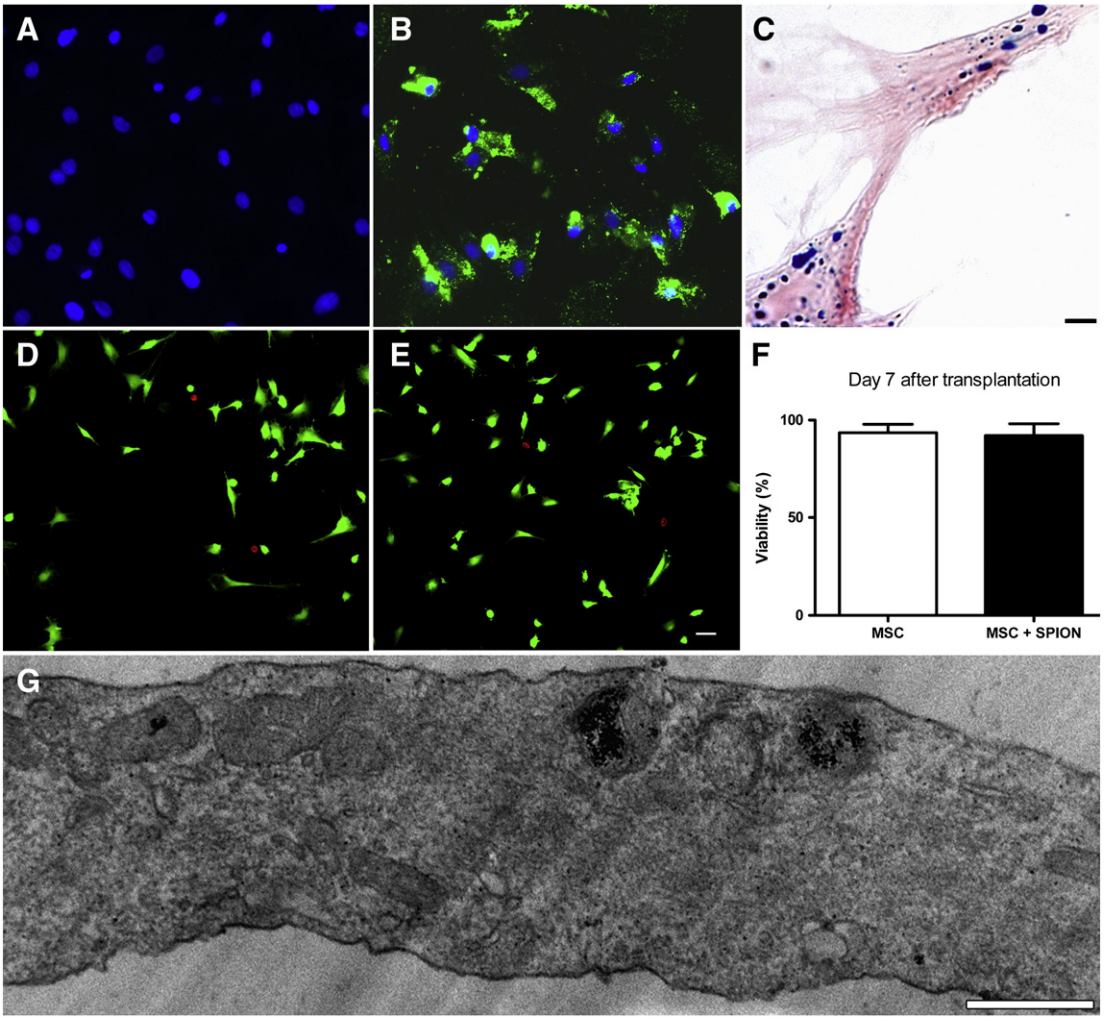

Figure 2 Uptake of SPION in cultured MSC. Micrographs showing anti-dextran staining in labeled MSC (B) but not in control non-labeled MSC (A). SPION appear blue within the MSC cytoplasm after Prussian blue staining (C). Analysis of cellular viability conducted with LIVE/DEAD kit (D–F) in samples of SPION-labeled (E) and non-labeled MSC (D). Graph shows results of live and dead cell quantifications (F). Cell viability was similar in both groups. Transmission electron microscopy evidenced the presence of numerous iron-containing vesicles (arrows) in the cytoplasm of MSC (G) (*$p<0.05$, Student's *t*-test). Scale bars: 20 μm. Scale bars: A, B, D and E = 20 μm; C = 10 μm; G = 200 nm.

20 min at 4 °C. The supernatant was collected, the protein concentration was determined using the Qubit-kit protein (Invitrogen) and 40 μg of total protein was loaded in 10% SDS-PAGE and transferred onto 0.2-μm nitrocellulose membranes (Amersham Biosciences, Pittsburgh, PA, USA). Membranes were blocked with 0.05% Tween-20 in PBS (PBS-T) containing 5% nonfat milk, for 1 h. After washing for 15 min in PBS-T, the membranes were incubated overnight with primary antibody in PBS-T at 4 °C with continuous shaking. Primary antibodies were directed against fibroblast growth factor-2 (FGF-2, 1:2000, Millipore) and α-tubulin (1:10,000, Sigma-Aldrich). After washing, the membranes were incubated at room temperature for 1 h with secondary horseradish peroxidase conjugated anti-mouse antibody (1:5000; Sigma) in PBS-T. The complex was revealed by chemiluminescence luminol reagent—ECL kit (Amersham Biosciences) and exposed to hyper film (Amersham Biosciences) for 30 min for FGF-2 and 5 min for α-tubulin. Scanning densitometry was employed to determine the relative intensity of the signal produced by protein expression levels and analyzed using Image J software (NIH). Loading controls were performed with an anti-α-tubulin antibody.

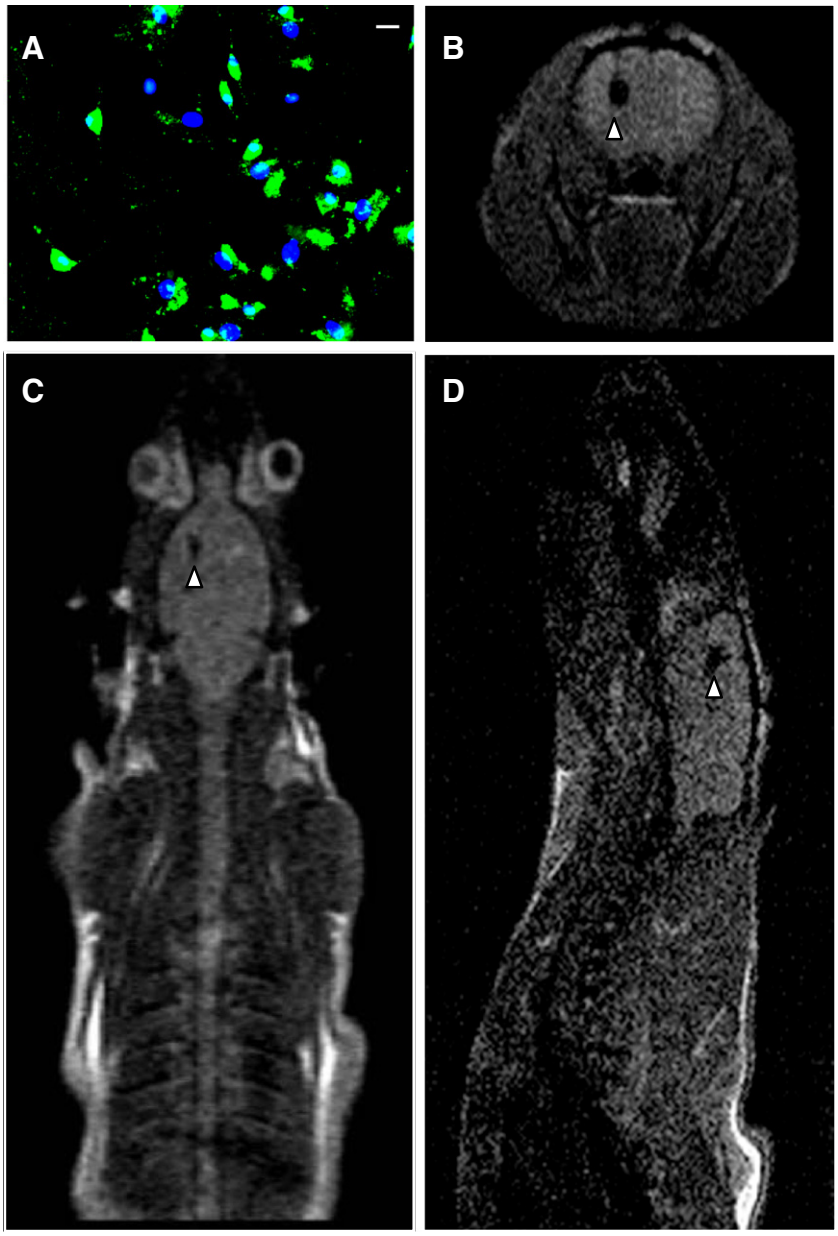

Figure 3 In vivo MR imaging. T2*-weighted images of a rat injected with SPION-labeled MSC. Anti-dextran staining using an aliquot of the injected SPION-labeled MSC confirmed the cell labeling (A). One hour after injection, a noticeable darkening appeared in the injected area, indicating the accumulation of labeled MSC within the lesioned and transplanted hemisphere (arrows in the coronal B, sagittal C and horizontal D planes) but not in the lesioned and untreated hemisphere. The signal remained primarily localized at the injection site. Scale bar: A = 20 μm.

Statistical analysis

Statistical analysis was performed by one-way ANOVA and the Tukey's multiple comparison post hoc test. Student's *t*-test was applied when indicated in the text (Graph Pad Prism 4 software). $P<0.05$ was considered as statistically significant.

Results

Neurodegeneration after QUIN

To define the therapeutic window after QUIN injections, we examined the chronology of cellular death after QUIN injections, using Fluoro-Jade C (FJ-C) as a tool for staining degenerating neurons. Striatal neurodegeneration was observed after the neurotoxic lesion (Figure 1B), and FJ-C positive cells were detected from day 1 to day 7 post-injection. Positive FJ-C staining was increased at earlier time points (1–3 d) following QUIN injection (Figure 1C). Because QUIN is an acute lesion, we considered that MSC transplantation immediately after lesion would provide a better effect.

In vitro characterization of SPION-labeled MSC

Studies from our group (Jasmin et al., 2010) and others have shown that labeling with SPION is feasible without affecting cell viability, proliferation, and differentiation ability (Arbab et al., 2004a, 2004b; Yang et al., 2011). The following experiments were designed to further investigate the SPION labeling. FITC-anti-dextran and Prussian blue showed intense staining of MSC, and confirmed the SPION uptake by these cells (Figures 2A–C). According to the live/dead assays, the number of surviving SPION-labeled MSC was similar to non-labeled MSC (Figures 2D–F). Thus, the next experiments were carried out with viable SPION-labeled MSC. Electron microscopy demonstrated that virtually all SPION particles were located inside the cells (Figure 2G). High-efficiency intracellular magnetic labeling would prevent loss of the label after MSC implantation.

In vivo tracking of SPION-labeled MSC

The next experiments were carried out to validate SPION-labeled MSC as a potential tool for MRI tracking. A rat received two bilateral striatal QUIN injections, followed by unilateral striatal injection of 10^6 SPION-labeled MSC and the contralateral *striatum* was injected with an equivalent volume of saline to exclude the possibility that bleeding after surgery could result in MRI signal changes and Prussian blue positive staining. One hour after transplantation, labeled MSC produced a visible and local hypointense MRI signal, while the contralateral lesioned *striatum* did not show signal alteration (Figure 3). This data indicated that internalized SPION induced sufficient cell MRI contrast to allow in vivo tracking of transplanted MSC. The MRI signal was visible at 1, 7, 14, 28, 42 and 60 days after implantation into the QUIN-lesioned *striatum* (Figure 4). Moreover, at day 7, a hypointense MRI signal was also found in the contralateral lesioned but not transplanted *striatum* (Figure 4). Histological evaluation with Prussian blue 60 days after transplantation also revealed the presence of iron in the *striata* of both hemispheres (Figure 5), supporting the MRI data. Most labeled cells were located next to blood vessels and lateral ventricles in both hemispheres. It is possible that cells attracted by inflammatory cytokines migrated from the injected to the contralateral hemisphere through the blood flow and/or the liquor. Brains injected with unlabeled MSC or the supernatant of SPION-labeled MSC after washing showed no MRI signal or Prussian blue staining (data not shown).

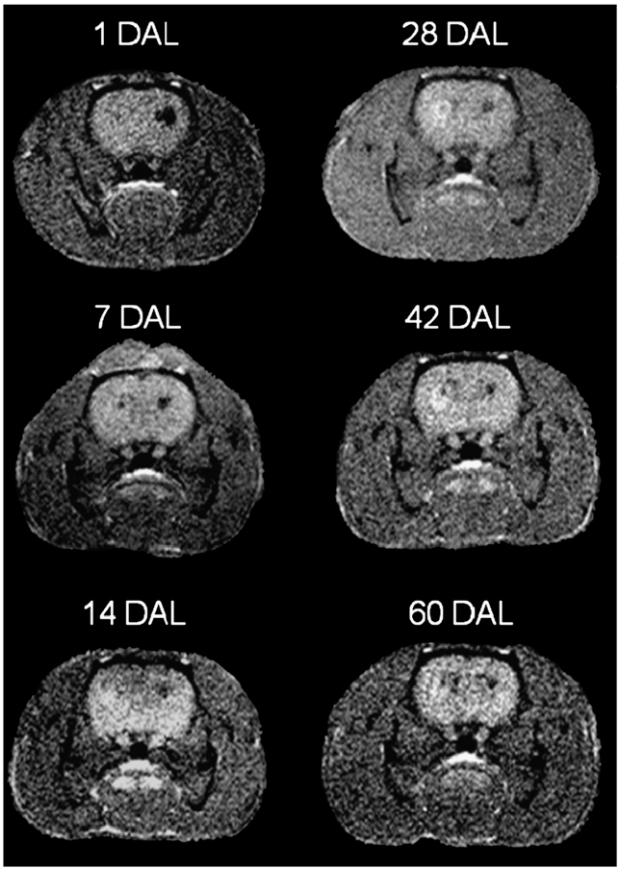

Figure 4 Long-term monitoring of SPION-labeled MSC. Coronal T2*-weighted images at different time points after delivery of SPION-labeled MSC. Hypointense signals (black spots) indicated the presence of the cells in all analyzed periods, and the signal was gradually reduced until 60 days after lesion (DAL). Seven days after cell injection, the black spots were also observed in the contralateral lesioned and non-transplanted *striatum*, and persisted for at least 60 DAL.

Neuroprotective effect of MSC transplantation

Analysis of neurodegeneration revealed significant reduction of FJ-C positive neurons in *striata* that received MSC transplants ($p<0.05$). Striatal neurodegeneration was significantly reduced at day 7 after MSC delivery, but this effect was not observed at day 1 (Figure 6).

Increased cell proliferation in the subventricular zone (SVZ) could constitute an alternative effect of MSC transplantation. To investigate the pattern of cell proliferation in the SVZ, we evaluated the number of cells expressing the

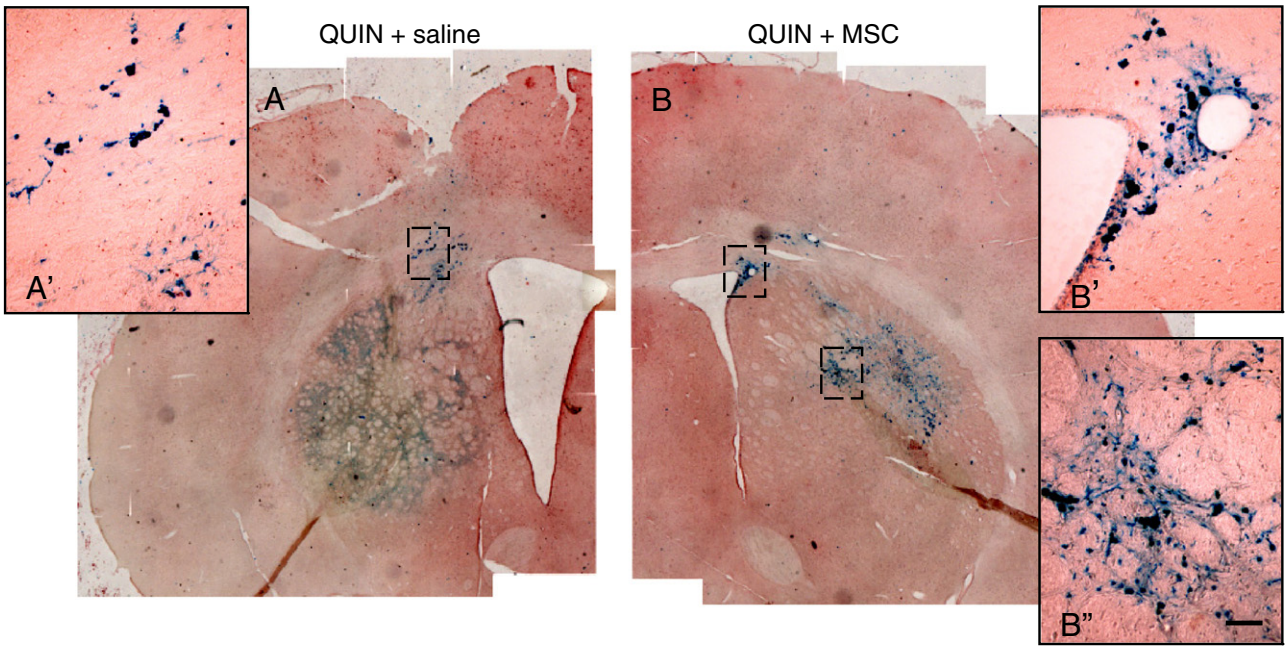

Figure 5 Prussian blue staining in the brain. Blue spots within both lesioned and transplanted (A and A′) and non-transplanted *striatum* (B, B′ and B″) showing the presence of SPION. Tissue counterstained with nuclear fast red. Magnification of the slides indicates the presence of SPION-labeled cells. Scale bar: A′, B′ and C′ 40 μm.

endogenous cell cycle marker Ki-67 in this region, and found no differences between rats transplanted with MSC and the saline control group at 7 days after injury. However, both groups showed increased numbers of Ki-67^{+} cells compared to unlesioned rats (Figure 7). This observation is in accordance with previous observations of cell proliferation enhancement in the SVZ ipsilateral to the QUIN lesioned striatum (Curtis et al., 2003; Tattersfield et al., 2004) and increased cell proliferation in the HD human brain (Curtis et al., 2003; Tattersfield et al., 2004).

Ventriculomegaly is one of the most prominent features of the progressive neurodegeneration in HD patients and in the QUIN model (Guncova et al., 2011). To investigate if MSC transplantation produced long-term effects in our model, we measured the degree of ventriculomegaly, which is an indication of striatal shrinkage. Nine months after transplantation, there was a significant enlargement of the ventricles in QUIN-saline rats compared to unlesioned rats. However, MSC treatment significantly decreased the enlargement of the ventricles (Figure 8). This effect was more evident and significant in the medial region, next to the MSC injection site ($p<0.05$). The significant reduction in ventriculomegaly 9 months after transplantation suggests that MSC transplantation can generate long-term positive effects after injury.

Increased levels of FGF-2 after MSC transplantation

We next investigated whether the effect of MSC on striatal cell survival at day 7 was associated with enhanced expression of fibroblast growth factor 2 (FGF-2). Immunoblotting analysis revealed that striatal FGF-2 expression is significantly reduced after QUIN injection, compared to unlesioned animals ($p<0.05$). On the other hand, MSC transplantation after QUIN injection can reverse this effect, since QUIN-MSC rats showed levels of striatal FGF-2 similar to those of unlesioned animals (Figure 9). Because brain-derived neurotrophic factor (BDNF) is believed to be an important regulator of neuronal survival in the *striatum*, we also analyzed its expression, and found no significant differences between the groups (Figure 9).

Discussion

MSC are known to play a therapeutic role in brain lesions, and can be safely cultured in vitro with no risk of malignant transformation (Bernardo et al., 2007; Uccelli et al., 2008). This is the first time that a therapeutic effect of MSC in HD with transplantation 1 h after QUIN lesions, and using a specific neurodegenerative marker, has been shown. We demonstrated that local MSC delivery has neuroprotective effects in a rat model of HD, leading to reduced striatal neurodegeneration and decreasing ventriculomegaly after QUIN injection. Furthermore, we demonstrated the feasibility of SPION labeling, and cells loaded with SPION were monitored in vivo in the *striata* of QUIN-lesioned rats.

We used FJ-C to evaluate the chronology of cellular death in the QUIN model and the effects of MSC on neurodegeneration. FJ-C is a good marker of degenerating neurons, and stains all types of cell death. Previous findings have indicated a peak at the third day, with reduced staining on the fifth day after lesion, using *Transferase Biotin-dUTP Nick End Labeling* (TUNEL) (Bordelon et al., 1999). We found a peak of FJ-C cells from 1 to 3 days after QUIN injection. This pattern might reflect the acute characteristic of QUIN-mediated lesion and the high sensitivity of FJ-C in acute neuronal injury, in contrast to its low sensitivity in delayed

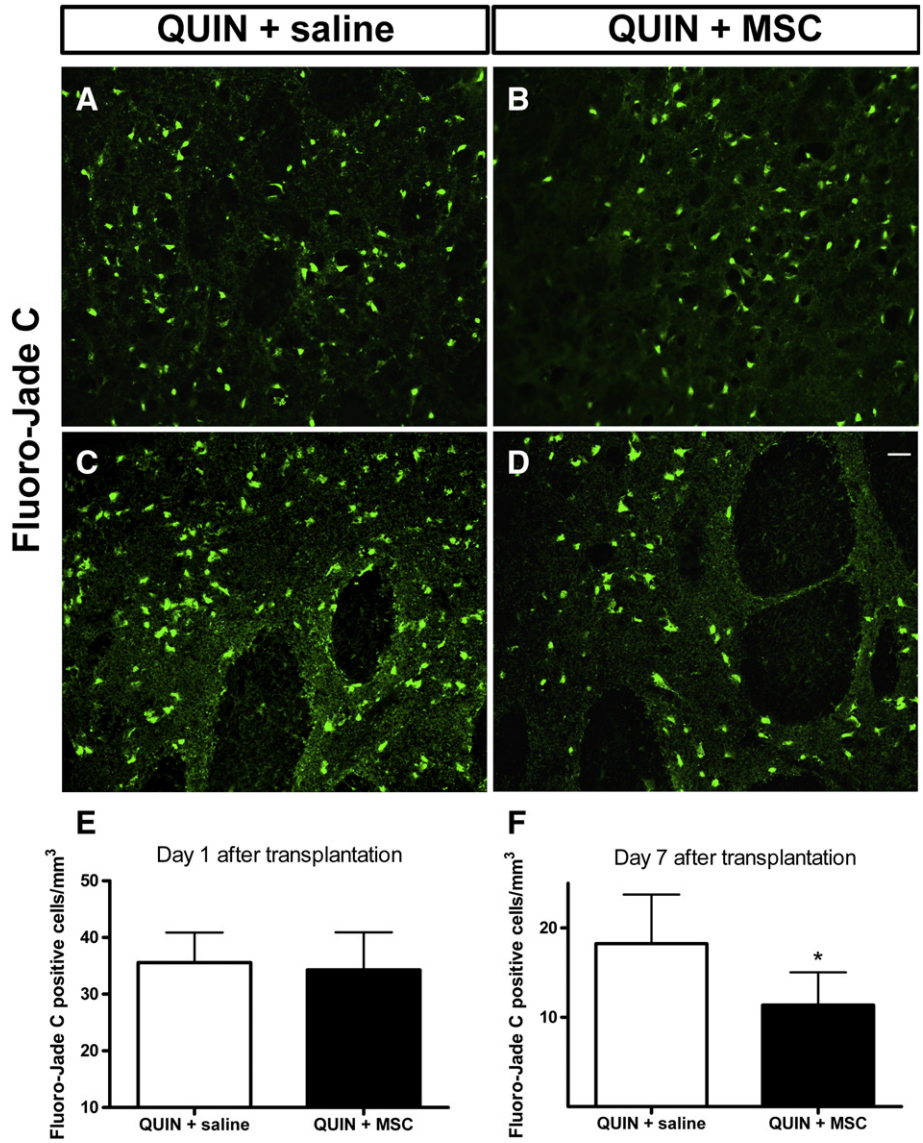

Figure 6 FJ-C positive cells after QUIN striatal injection (A–D). There was no difference in the striatal neurodegeneration of non-transplanted (A) and transplanted (B) groups at day 1 after QUIN injection. However, a larger number of degenerating neurons was found in saline-injected *striata* (C) compared to MSC-transplanted *striata* (D) 7 days after surgery. Graphs show quantification of FJ-C positive cells in *striata* (E–F). In transplanted rats, we observed no differences in the number of FJ-C positive neurons at 1 d post-lesion (E), but 7 d following surgery the striatal MSC transplantation significantly reduced the neurodegeneration (F) (*$p<0.05$, Student's *t*-test). Scale bar: A–D = 20 μm.

assessment of damage (Lee et al., 2010). Because most cells die in the first days after QUIN, we tested the neuroprotective potential of MSC transplanted early after the insult. The first hours might be critical in saving damaged tissue, since DNA fragmentation that indicates cellular death is detected 1 h after QUIN (Dure et al., 1995). It is possible that a similar effect would be achieved if patients could be treated in the initial phase of the disease.

We found significantly reduced striatal neurodegeneration in lesioned rats 7 days after transplantation. This result may be related to a paracrine effect of MSC, which might serve to inhibit the progression of damage, as reviewed by others (Le Blanc and Ringden, 2007; Uccelli et al., 2007). MSC are known to release neurotrophic factors that are important for neuronal survival and growth (Caplan and Dennis, 2006). Moreover, numerous reports have revealed that MSC have immunomodulatory properties, including suppression of T-cell proliferation (Aggarwal and Pittenger, 2005; Di Nicola et al., 2002), inhibition of resting natural killer cytotoxic activity (Liu et al., 2009; Sotiropoulou et al., 2006) and microglial activation (Lee et al., 2009).

It is not known exactly when the improvements start after MSC transplantation. We found no differences in the striatal neurodegeneration of transplanted and non-transplanted lesioned rats 24 h after the transplantation procedure. Thus, a gap might be necessary between cell transplantation and detectable neuroprotective effects. Since MSC-mediated neuroprotection is related to their anti-inflammatory effects and secretion of growth factors, 24 h may not be sufficient for MSC to produce substantial amounts of soluble factors

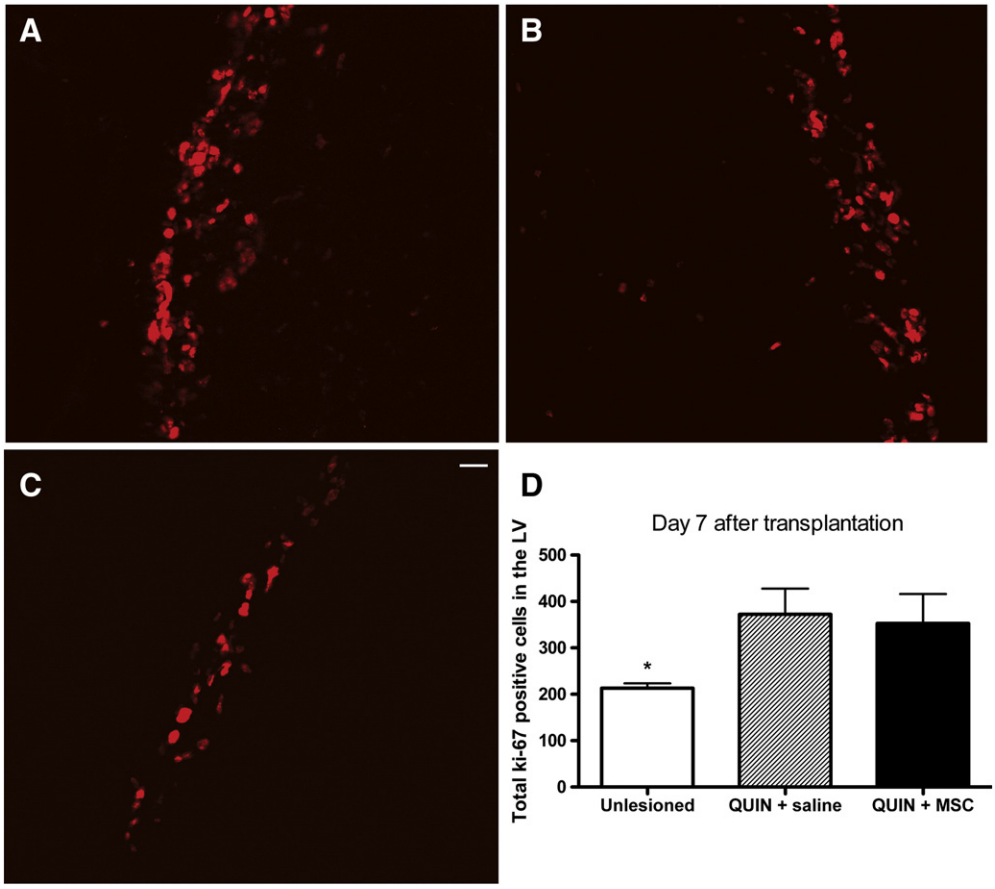

Figure 7 Cell proliferation analysis in the SVZ. Micrographs show Ki-67^{+} cells in the SVZ of QUIN-treated (A), QUIN-untreated (B), and unlesioned (C) rats. Quantitative analysis (D) showed that both treated and untreated animals had significantly enhanced SVZ proliferation (*$p<0.05$) compared to unlesioned animals, but that transplantation per se did not affect SVZ proliferation (LV, lateral ventricle) (*$p<0.05$, one-way ANOVA followed by Tukey's test). Scale bar: A–C = 20 μm.

and/or be stimulated by the microenvironment to produce further improvement. It is also possible that MSC transplantation protected the partially integrated tissue and neurons that undergo secondary death, but not neurons that die rapidly after QUIN injection. Another potential explanation for the absence of neuroprotection 24 h after QUIN lesion might be that transplanted MSC act through interference with a progressive inflammatory process that begins after the initial damage. Our group has recently shown that cell therapy has neuroprotective effects related to reduced microglial activation in hypoxic–ischemic brain damage (Pimentel-Coelho et al., 2010) and reduced astrogliosis after optic nerve crush (Zaverucha-do-Valle et al., 2011). These data corroborate the idea that stress signals in the lesioned tissue can induce MSC to produce a more anti-inflammatory phenotype (Ohtaki et al., 2008). Astrocytes and microglia responses are characteristic in HD models and patients. It was previously shown that in QUIN-lesioned rats, the density of reactive astrogliosis corresponds to the local severity of the neurodegenerative process (Guncova et al., 2011) and in HD patients the microglial activation correlates with severity (Pavese et al., 2006). Thus, the inflammatory processes after MSC transplantation in HD models remain an important issue for further investigation.

In HD, the cerebral tissue loss is compensated by the enhancement of the ventricular area, and ventriculomegaly is indicative of a progressive neurodegeneration (Guncova et al., 2011). We found reduced ventriculomegaly 9 months after QUIN injection and MSC transplantation. This finding is in accordance with the previous data that late transplantation of MSC leads to reversal of striatal atrophy (Amin et al., 2008), and suggests that the neuroprotective effects of MSC are not transitory. The observed neuroprotective effect of MSC transplantation is also in accordance with previous evidences that bone marrow stem cell transplantation leads to improved motor skills in animal models of HD (Edalatmanesh et al., 2010; Jiang et al., 2011; Lescaudron et al., 2003).

We observed a discrete enhancement of FGF-2, but not BDNF striatal expression 7 days after lesion in treated rats. FGF-2 is expressed constitutively in the brain (Baird and Walicke, 1989), and can be secreted by cells of the damaged tissue (Reuss and von Bohlen und Halbach, 2003). FGF-2 is neuroprotective in many neurological diseases (Reuss and von Bohlen und Halbach, 2003) and after ischemia it prevents neuronal death in a dose-dependent manner (Nakata et al., 1993). It is known that FGF-2 can reduce cellular death in striatal cultures of the R6/2 transgenic model of HD (K. Jin et al., 2005), and intracerebral injection

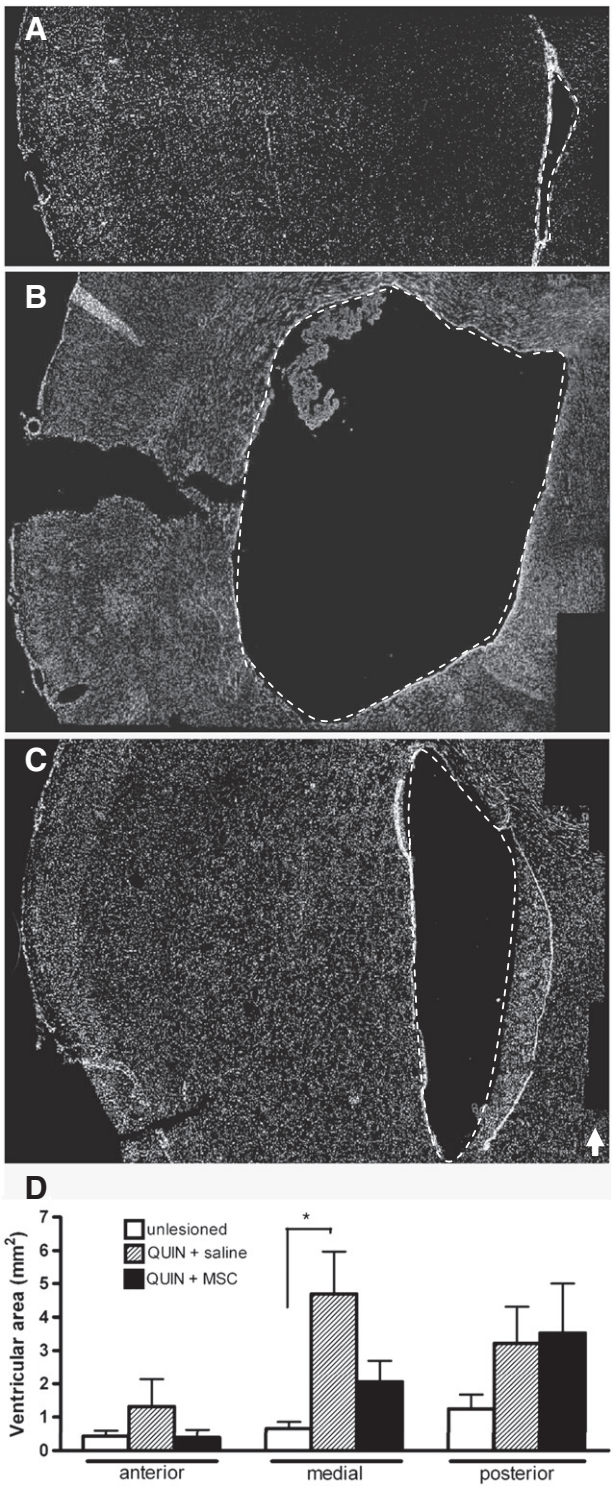

Figure 8 Ventriculomegaly analysis to assess striatal shrinkage. Photomontage of brain coronal sections illustrates an unlesioned brain (A) and the pronounced enlargement of lateral ventricles in untreated (B) rats compared to MSC transplanted animals (C), 9 months after lesion. The dashed lines delineate the ventricular area and the arrow indicates the brain midline (A–C). Graph shows measurements of the ventricular area in coronal sections of different brain rostrocaudal levels (D). Ventriculomegaly is significantly less severe in the medial region of treated animals compared to the untreated group (*$p<0.05$, one-way ANOVA followed by Tukey's test). 1.

of this factor leads to functional improvements in R6/2 mice (K. Jin et al., 2005). Our group has previously shown that bone-marrow mononuclear cells can increase neuroprotection, neuroregeneration, and FGF-2 expression in a model of optic nerve crush (Zaverucha-do-Valle et al., 2011). Thus, it is possible that the neuroprotection after QUIN injection is, at least in part, mediated by FGF-2 secreted by transplanted MSC, but it is unlikely that this is the only factor to play a role. FGF-2 activates a range of signal transduction pathways, among which the phosphatidylinositol 3′-kinase/Akt pathway is related to cell survival (K. Jin et al., 2005).

We observed a considerable and significant enhancement in SVZ cell proliferation after QUIN injection, in both transplanted and non-transplanted rats. Many investigators have described enhanced proliferation and/or altered SVZ migration in response to brain lesions, including HD (Curtis et al., 2003; Moraes et al., 2009), ischemia (Liu et al., 1998), Alzheimer's (K. Jin et al., 2004) and Parkinson's (Zhao et al., 2003) diseases (Batista et al., 2006; Goings et al., 2004), giving rise to the possibility of cell replacement from endogenous precursors (Arvidsson et al., 2002). The observed proliferative response in the SVZ of QUIN-lesioned rats was previously correlated with stem cell-factor release from the lesioned *striata*, which activates the *c-kit* receptor in neural stem cells and a signaling pathway associated with cellular proliferation and migration (Bantubungi et al., 2008). Although we did not find proliferative modulation associated with MSC transplantation in the SVZ, our analysis was time-limited, and we do not reject the hypothesis that MSC can affect the SVZ microenvironment. One possibility is that the newly generated cells in the SVZ survive longer after MSC transplantation. In accordance with this view, previous findings showed that MSC can enhance neuroblast proliferation and differentiation in the *striata* of R6/2 mice (Lin et al., 2011). Indeed, we observed Ki-67-positive cells in the *striata* of both transplanted and non-transplanted QUIN-lesioned rats (data not shown) and it is possible that some of these cells were neuroblasts.

Previous studies demonstrated SPION-labeling in a variety of human (Niemeyer et al., 2010; Song et al., 2007) and animal (Rice et al., 2007; Zhu et al., 2007) stem cells. We used SPION to track MSC in the QUIN model. SPION were internalized in MSC without affecting cellular viability. These data corroborate previous findings of SPION biosafety (Arbab et al., 2003) and viability maintenance 3 to 7 days after labeling, even using high concentrations of SPION (Jasmin et al., 2010). The MRI signal was generated by labeled cells and remained restricted to the injection site 1 h after transplantation. MRI signals lasted for at least 60 days, and it is likely that it gradually disappeared due to cell proliferation. Previous data showed that inhibition of cell proliferation mediated by Mitomycin-C reduces SPION loss from labeled MSC (Jasmin et al., 2010).

Our in vivo tracking of SPION-labeled MSC suggested migration from the injection site to the contralateral lesioned *striatum*. MSC migration between hemispheres was described earlier (Li et al., 2011; Wang et al., 2002). Because stained cells were located next to blood vessels and cerebral ventricles, we speculate that they migrated through the blood flow and/or the liquor. MSC migration has been associated with SDF-1/CXCR4 pathway (Tyndall et al., 2007), fractalcin and its receptor CX3CR1 (Ji et al., 2004) (Sordi et al., 2005), TNF-α,

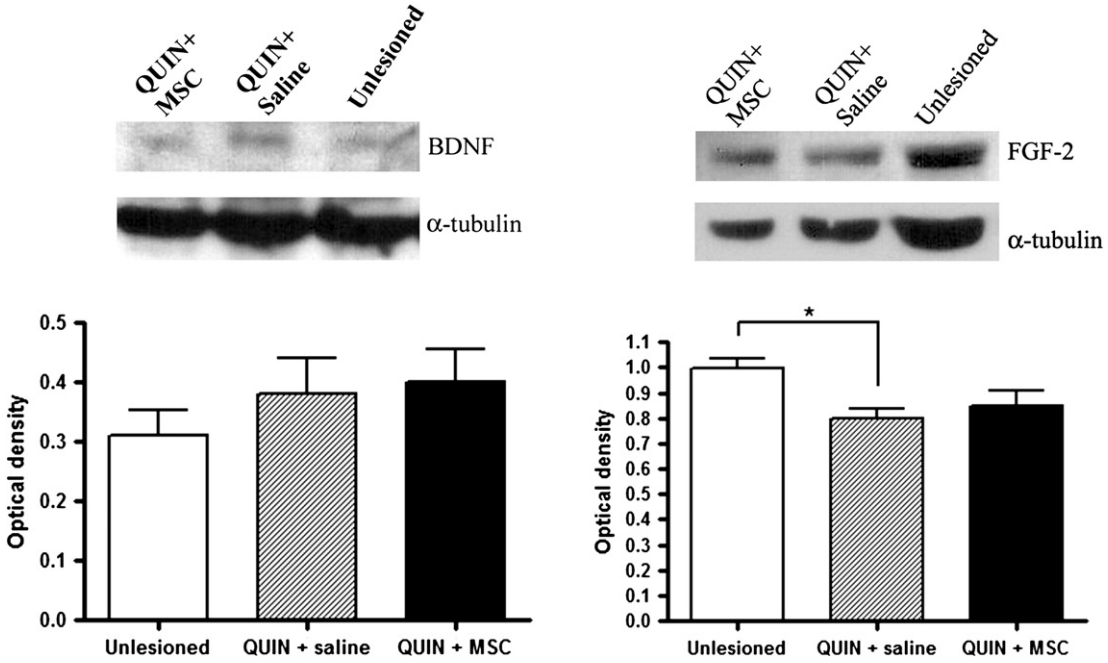

Figure 9 Analysis of BDNF and FGF2 expression levels. The normal *striata* express both neurotrophic factors. In both treated and untreated lesioned animals, BDNF expression seems to increase in relation to unlesioned animals, but the difference is not significant between the groups. In the MSC-treated group, the level of FGF-2 expression is significantly more pronounced than in the saline group when both are compared to unlesioned animals (*$p<0.05$, one-way ANOVA followed by Tukey's test).

and MCP-1 (Fu et al., 2009). MSC local permanence seems not to require persistent integration. The "touch and go effect" (Uccelli et al., 2008) has been discussed as a potential therapeutic characteristic of MSC, which includes induction of a neuroprotective microenvironment with subsequent clearance of the lesioned tissue.

In the present study, we showed that acute MSC transplantation can produce long-term benefits in the QUIN model of HD, and it is possible that neuroprotection occurs in other neurological diseases in which excitotoxicity plays a role. Further in vivo monitoring of transplanted cells will be instrumental for a better understanding of their migratory dynamics and to improve clinical transplantation strategies.

Acknowledgments

This study was supported by grants from the Ministry of Health (MS/SCTIE/DECIT), from Conselho Nacional de Desenvolvimento Científico e Tecnológico (CNPq), Instituto Nacional de Ciência e Tecnologia de Biologia Estrutural e Bioimagem (Inbeb), Coordenação de Aperfeiçoamento de Pessoal de Nível Superior (CAPES) and Fundação Carlos Chagas Filho de Amparo à Pesquisa do Estado do Rio de Janeiro (FAPERJ). The authors thank Suelen Sério and Felipe Marins for technical assistance, and Janet W. Reid for editing the manuscript.

References

Aggarwal, S., Pittenger, M.F., 2005. Human mesenchymal stem cells modulate allogeneic immune cell responses. Blood 105 (4), 1815–1822.

Amin, E.M., Reza, B.A., Morteza, B.R., Maryam, M.M., Ali, M., Zeinab, N., 2008. Microanatomical evidences for potential of mesenchymal stem cells in amelioration of striatal degeneration. Neurol. Res. 30 (10), 1086–1090.

Arbab, A.S., Bashaw, L.A., Miller, B.R., Jordan, E.K., Bulte, J.W., Frank, J.A., 2003. Intracytoplasmic tagging of cells with ferumoxides and transfection agent for cellular magnetic resonance imaging after cell transplantation: methods and techniques. Transplantation 76 (7), 1123–1130.

Arbab, A.S., Yocum, G.T., Kalish, H., Jordan, E.K., Anderson, S.A., Khakoo, A.Y., Frank, J.A., 2004a. Efficient magnetic cell labeling with protamine sulfate complexed to ferumoxides for cellular MRI. Blood 104 (4), 1217–1223.

Arbab, A.S., Yocum, G.T., Wilson, L.B., Parwana, A., Jordan, E.K., Kalish, H., Frank, J.A., 2004b. Comparison of transfection agents in forming complexes with ferumoxides, cell labeling efficiency, and cellular viability. Mol. Imaging 3 (1), 24–32.

Arvidsson, A., Collin, T., Kirik, D., Kokaia, Z., Lindvall, O., 2002. Neuronal replacement from endogenous precursors in the adult brain after stroke. Nat. Med. 8 (9), 963–970.

Baird, A., Walicke, P.A., 1989. Fibroblast growth factors. Br. Med. Bull. 45 (2), 438–452.

Bantubungi, K., Blum, D., Cuvelier, L., Wislet-Gendebien, S., Rogister, B., Brouillet, E., Schiffmann, S.N., 2008. Stem cell factor and mesenchymal and neural stem cell transplantation in a rat model of Huntington's disease. Mol. Cell. Neurosci. 37 (3), 454–470.

Batista, C.M., Kippin, T.E., Willaime-Morawek, S., Shimabukuro, M.K., Akamatsu, W., van der Kooy, D., 2006. A progressive and cell non-autonomous increase in striatal neural stem cells in the Huntington's disease R6/2 mouse. J. Neurosci. 26 (41), 10452–10460.

Bernardo, M.E., Zaffaroni, N., Novara, F., Cometa, A.M., Avanzini, M.A., Moretta, A., Locatelli, F., 2007. Human bone marrow derived mesenchymal stem cells do not undergo transformation after long-term in vitro culture and do not exhibit telomere maintenance mechanisms. Cancer Res. 67 (19), 9142–9149.

Bordelon, Y.M., Mackenzie, L., Chesselet, M.F., 1999. Morphology and compartmental location of cells exhibiting DNA damage

after quinolinic acid injections into rat striatum. J. Comp. Neurol. 412 (1), 38–50.
Caplan, A.I., Dennis, J.E., 2006. Mesenchymal stem cells as trophic mediators. J. Cell. Biochem. 98 (5), 1076–1084.
Cowan, C.M., Raymond, L.A., 2006. Selective neuronal degeneration in Huntington's disease. Curr. Top. Dev. Biol. 75, 25–71.
Curtis, M.A., Penney, E.B., Pearson, A.G., van Roon-Mom, W.M., Butterworth, N.J., Dragunow, M., Faull, R.L., 2003. Increased cell proliferation and neurogenesis in the adult human Huntington's disease brain. Proc. Natl. Acad. Sci. U. S. A. 100 (15), 9023–9027.
Di Nicola, M., Carlo-Stella, C., Magni, M., Milanesi, M., Longoni, P.D., Matteucci, P., Gianni, A.M., 2002. Human bone marrow stromal cells suppress T-lymphocyte proliferation induced by cellular or nonspecific mitogenic stimuli. Blood 99 (10), 3838–3843.
Dure, L.S. 4th, Wiess, S., Standaert, D.G., Rudolf, G., Testa, C.M., Young, A.B., 1995. DNA fragmentation and immediate early gene expression in rat striatum following quinolinic acid administration. Exp. Neurol. 133 (2), 207–214.
Edalatmanesh, M.A., Matin, M.M., Neshati, Z., Bahrami, A.R., Kheirabadi, M., 2010. Systemic transplantation of mesenchymal stem cells can reduce cognitive and motor deficits in rats with unilateral lesions of the neostriatum. Neurol. Res. 32 (2), 166–172.
Estrada Sanchez, A.M., Mejia-Toiber, J., Massieu, L., 2008. Excitotoxic neuronal death and the pathogenesis of Huntington's disease. Arch. Med. Res. 39 (3), 265–276.
Fu, X., Han, B., Cai, S., Lei, Y., Sun, T., Sheng, Z., 2009. Migration of bone marrow-derived mesenchymal stem cells induced by tumor necrosis factor-alpha and its possible role in wound healing. Wound Repair Regen. 17 (2), 185–191.
Goings, G.E., Sahni, V., Szele, F.G., 2004. Migration patterns of subventricular zone cells in adult mice change after cerebral cortex injury. Brain Res. 996 (2), 213–226.
Guncova, I., Latr, I., Mazurova, Y., 2011. The neurodegenerative process in a neurotoxic rat model and in patients with Huntington's disease: histopathological parallels and differences. Acta Histochem. 113 (8), 783–792.
Jasmin, Torres, A.L., Nunes, H.M., Passipieri, J.A., Jelicks, L.A., Gasparetto, E.L., Mendez-Otero, R., 2010. Optimized labeling of bone marrow mesenchymal cells with superparamagnetic iron oxide nanoparticles and in vivo visualization by magnetic resonance imaging. J. Nanobiotechnol. 9, 4.
Ji, J.F., He, B.P., Dheen, S.T., Tay, S.S., 2004. Interactions of chemokines and chemokine receptors mediate the migration of mesenchymal stem cells to the impaired site in the brain after hypoglossal nerve injury. Stem Cells 22 (3), 415–427.
Jiang, Y., Lv, H., Huang, S., Tan, H., Zhang, Y., Li, H., 2011. Bone marrow mesenchymal stem cells can improve the motor function of a Huntington's disease rat model. Neurol. Res. 33 (3), 331–337.
Jin, H.K., Carter, J.E., Huntley, G.W., Schuchman, E.H., 2002. Intracerebral transplantation of mesenchymal stem cells into acid sphingomyelinase-deficient mice delays the onset of neurological abnormalities and extends their life span. J. Clin. Invest. 109 (9), 1183–1191.
Jin, K., Peel, A.L., Mao, X.O., Xie, L., Cottrell, B.A., Henshall, D.C., Greenberg, D.A., 2004. Increased hippocampal neurogenesis in Alzheimer's disease. Proc. Natl. Acad. Sci. U. S. A. 101 (1), 343–347.
Jin, K., LaFevre-Bernt, M., Sun, Y., Chen, S., Gafni, J., Crippen, D., Ellerby, L.M., 2005. FGF-2 promotes neurogenesis and neuroprotection and prolongs survival in a transgenic mouse model of Huntington's disease. Proc. Natl. Acad. Sci. U. S. A. 102 (50), 18189–18194.
Jung, C.W., Jacobs, P., 1995. Physical and chemical properties of superparamagnetic iron oxide MR contrast agents: ferumoxides, ferumoxtran, ferumoxsil. Magn. Reson. Imaging 13 (5), 661–674.
Kassis, I., Grigoriadis, N., Gowda-Kurkalli, B., Mizrachi-Kol, R., Ben-Hur, T., Slavin, S., Karussis, D., 2008. Neuroprotection and immunomodulation with mesenchymal stem cells in chronic experimental autoimmune encephalomyelitis. Arch. Neurol. 65 (6), 753–761.
Le Blanc, K., Ringden, O., 2007. Immunomodulation by mesenchymal stem cells and clinical experience. J. Intern. Med. 262 (5), 509–525.
Lee, J.K., Jin, H.K., Bae, J.S., 2009. Bone marrow-derived mesenchymal stem cells reduce brain amyloid-beta deposition and accelerate the activation of microglia in an acutely induced Alzheimer's disease mouse model. Neurosci. Lett. 450 (2), 136–141.
Lee, J.K., Jin, H.K., Endo, S., Schuchman, E.H., Carter, J.E., Bae, J.S., 2010. Intracerebral transplantation of bone marrow-derived mesenchymal stem cells reduces amyloid-beta deposition and rescues memory deficits in Alzheimer's disease mice by modulation of immune responses. Stem Cells 28 (2), 329–343.
Lescaudron, L., Unni, D., Dunbar, G.L., 2003. Autologous adult bone marrow stem cell transplantation in an animal model of Huntington's disease: behavioral and morphological outcomes. Int. J. Neurosci. 113 (7), 945–956.
Li, J.M., Zhu, H., Lu, S., Liu, Y., Li, Q., Ravenscroft, P., Qin, C., 2011. Migration and differentiation of human mesenchymal stem cells in the normal rat brain. Neurol. Res. 33 (1), 84–92.
Lin, Y.T., Chern, Y., Shen, C.K., Wen, H.L., Chang, Y.C., Li, H., Hsieh-Li, H.M., 2011. Human mesenchymal stem cells prolong survival and ameliorate motor deficit through trophic support in Huntington's disease mouse models. PLoS One 6 (8), e22924.
Liu, J., Solway, K., Messing, R.O., Sharp, F.R., 1998. Increased neurogenesis in the dentate gyrus after transient global ischemia in gerbils. J. Neurosci. 18 (19), 7768–7778.
Liu, F., Schafer, D.P., McCullough, L.D., 2009. TTC, fluoro-Jade B and NeuN staining confirm evolving phases of infarction induced by middle cerebral artery occlusion. J. Neurosci. Methods 179 (1), 1–8.
Moraes, L., de Moraes Mello, L.E., Shimabukuro, M.K., de Castro Batista, C.M., Mendez-Otero, R., 2009. Lack of association between PSA-NCAM expression and migration in the rostral migratory stream of a Huntington's disease transgenic mouse model. Neuropathology 29 (2), 140–147.
Nakata, N., Kato, H., Kogure, K., 1993. Protective effects of basic fibroblast growth factor against hippocampal neuronal damage following cerebral ischemia in the gerbil. Brain Res. 605 (2), 354–356.
Niemeyer, M., Oostendorp, R.A., Kremer, M., Hippauf, S., Jacobs, V.R., Baurecht, H., Beer, A.J., 2010. Non-invasive tracking of human haemopoietic CD34(+) stem cells in vivo in immunodeficient mice by using magnetic resonance imaging. Eur. Radiol. 20 (9), 2184–2193.
Ohtaki, H., Ylostalo, J.H., Foraker, J.E., Robinson, A.P., Reger, R.L., Shioda, S., Prockop, D.J., 2008. Stem/progenitor cells from bone marrow decrease neuronal death in global ischemia by modulation of inflammatory/immune responses. Proc. Natl. Acad. Sci. U. S. A. 105 (38), 14638–14643.
Pavese, N., Gerhard, A., Tai, Y.F., Ho, A.K., Turkheimer, F., Barker, R.A., Piccini, P., 2006. Microglial activation correlates with severity in Huntington disease: a clinical and PET study. Neurology 66 (11), 1638–1643.
Pimentel-Coelho, P.M., Magalhaes, E.S., Lopes, L.M., deAzevedo, L.C., Santiago, M.F., Mendez-Otero, R., 2010. Human cord blood transplantation in a neonatal rat model of hypoxic–ischemic brain damage: functional outcome related to neuroprotection in the striatum. Stem Cells Dev. 19 (3), 351–358.
Reuss, B., von Bohlen und Halbach, O., 2003. Fibroblast growth factors and their receptors in the central nervous system. Cell Tissue Res. 313 (2), 139–157.
Rice, H.E., Hsu, E.W., Sheng, H., Evenson, D.A., Freemerman, A.J., Safford, K.M., Johnson, G.A., 2007. Superparamagnetic iron

oxide labeling and transplantation of adipose-derived stem cells in middle cerebral artery occlusion-injured mice. AJR Am. J. Roentgenol. 188 (4), 1101–1108.

Rogers, W.J., Meyer, C.H., Kramer, C.M., 2006. Technology insight: in vivo cell tracking by use of MRI. Nat. Clin. Pract. Cardiovasc. Med. 3 (10), 554–562.

Sieradzan, K.A., Mann, D.M., 2001. The selective vulnerability of nerve cells in Huntington's disease. Neuropathol. Appl. Neurobiol. 27 (1), 1–21.

Song, M., Moon, W.K., Kim, Y., Lim, D., Song, I.C., Yoon, B.W., 2007. Labeling efficacy of superparamagnetic iron oxide nanoparticles to human neural stem cells: comparison of ferumoxides, monocrystalline iron oxide, cross-linked iron oxide (CLIO)-NH2 and tat-CLIO. Korean J. Radiol. 8 (5), 365–371.

Sordi, V., Malosio, M.L., Marchesi, F., Mercalli, A., Melzi, R., Giordano, T., Piemonti, L., 2005. Bone marrow mesenchymal stem cells express a restricted set of functionally active chemokine receptors capable of promoting migration to pancreatic islets. Blood 106 (2), 419–427.

Sotiropoulou, P.A., Perez, S.A., Gritzapis, A.D., Baxevanis, C.N., Papamichail, M., 2006. Interactions between human mesenchymal stem cells and natural killer cells. Stem Cells 24 (1), 74–85.

Subramaniam, S., Sixt, K.M., Barrow, R., Snyder, S.H., 2009. Rhes, a striatal specific protein, mediates mutant-huntingtin cytotoxicity. Science 324 (5932), 1327–1330.

Tattersfield, A.S., Croon, R.J., Liu, Y.W., Kells, A.P., Faull, R.L., Connor, B., 2004. Neurogenesis in the striatum of the quinolinic acid lesion model of Huntington's disease. Neuroscience 127 (2), 319–332.

The Huntington's Disease Collaborative Research Group, 1993. A novel gene containing a trinucleotide repeat that is expanded and unstable on Huntington's disease chromosomes. Cell 72 (6), 971–983.

Tyndall, A., Walker, U.A., Cope, A., Dazzi, F., De Bari, C., Fibbe, W., Feldmann, M., 2007. Immunomodulatory properties of mesenchymal stem cells: a review based on an interdisciplinary meeting held at the Kennedy Institute of Rheumatology Division, London, UK, 31 October 2005. Arthritis Res. Ther. 9 (1), 301.

Uccelli, A., Pistoia, V., Moretta, L., 2007. Mesenchymal stem cells: a new strategy for immunosuppression? Trends Immunol. 28 (5), 219–226.

Uccelli, A., Mancardi, G., Chiesa, S., 2008. Is there a role for mesenchymal stem cells in autoimmune diseases? Autoimmunity 41 (8), 592–595.

Wang, L., Li, Y., Chen, J., Gautam, S.C., Zhang, Z., Lu, M., Chopp, M., 2002. Ischemic cerebral tissue and MCP-1 enhance rat bone marrow stromal cell migration in interface culture. Exp. Hematol. 30 (7), 831–836.

Yang, C.Y., Hsiao, J.K., Tai, M.F., Chen, S.T., Cheng, H.Y., Wang, J.L., Liu, H.M., 2011. Direct labeling of hMSC with SPIO: the long-term influence on toxicity, chondrogenic differentiation capacity, and intracellular distribution. Mol. Imaging Biol. 13 (3), 443–451.

Zaverucha-do-Valle, C., Gubert, F., Bargas-Rega, M., Coronel, J.L., Mesentier-Louro, L.A., Mencalha, A., Mendez-Otero, R., 2011. Bone marrow mononuclear cells increase retinal ganglion cell survival and axon regeneration in the adult rat. Cell Transplant. 20 (3), 391–406.

Zhao, M., Momma, S., Delfani, K., Carlen, M., Cassidy, R.M., Johansson, C.B., Janson, A.M., 2003. Evidence for neurogenesis in the adult mammalian substantia nigra. Proc. Natl. Acad. Sci. U. S. A. 100 (13), 7925–7930.

Zhu, W., Li, X., Tang, Z., Zhu, S., Qi, J., Wei, L., Lei, H., 2007. Superparamagnetic iron oxide labeling of neural stem cells and 4.7 T MRI tracking in vivo and in vitro. J. Huazhong Univ. Sci. Technolog. Med. Sci. 27 (1), 107–110.